Motion of a nano-ellipsoid in a cylindrical vessel flow: Brownian and hydrodynamic interactions.

N. Ramakrishnan[1,*] Y. Wang[2,*]† D. M. Eckmann[1,3] P. S. Ayyaswamy[2] R. Radhakrishnan[1,4,5]‡

[*]These authors contributed equally

[1]Department of Bioengineering, University of Pennsylvania, Philadelphia, PA-19104

[2]Department of Mechanical Engineering and Applied Mechanics, University of Pennsylvania, Philadelphia, PA-19104

[3]Department of Anesthesiology and Critical Care, University of Pennsylvania, Philadelphia, PA-19104

[4]Department of Chemical and Biomolecular Engineering, University of Pennsylvania, Philadelphia, PA-19104

[5]Department of Biochemistry and Biophysics, University of Pennsylvania, Philadelphia, PA-19104

(Received xx; revised xx; accepted xx)

S1. FHD data for ellipsoidal particles of different aspect ratio

In this section, we present data from FHD simulations for ellipsoidal particles, with five different aspect ratios $\varepsilon = 0.5$, 1.0, 1.5, 2.0, and 5.0, placed at three different locations, inside a cylindrical tube of diameter $D = 5\,\mu$m and length $L = 40\,\mu$m.

In each of the panel plots presented here, *columns from left to right* correspond to

(i) the velocity distribution, $P(U_\alpha)\,dU_\alpha$.
(ii) time series of the scaled averaged translational temperature, $T_\alpha^{(\mathrm{t})}/T$, and rotational temperature, $T_\alpha^{(\mathrm{r})}/T$.
(iii) time series of the VACF, $C_{U_\alpha}(t)$, and AVACF $C_{\Omega_\alpha}(t)$.
(iv) the mean squared displacement (MSD), $\langle \Delta X_{\alpha\alpha}(t)\rangle$.

Rows from top to bottom correspond to the above mentioned measures computed for the

(i) translational component along the x direction,
(ii) translational component along the y direction,
(iii) translational component along the z direction,
(iv) rotational component along the 1 direction,
(v) rotational component along the 2 direction, and
(vi) rotational component along the 3 direction.

The parameters corresponding to Figs. S1.1- S1.15 are shown in Table. S1.1.

† Presently at Center for Applied Mathematics, Tianjin University, Tianjin, China, 300072.
‡ Email address for correspondence: rradhak@seas.upenn.edu

Figure	ε	a (in nm)	$\widetilde{h}$
Fig. S1.1	0.5	288.4	7.667
Fig. S1.2	0.5	288.4	1.0
Fig. S1.3	0.5	288.4	0.2
Fig. S1.4	1.0	457.9	7.962
Fig. S1.5	1.0	457.9	1.0
Fig. S1.6	1.0	457.9	0.2
Fig. S1.7	1.5	600.0	11.5
Fig. S1.8	1.5	600.0	1.0
Fig. S1.9	1.5	600.0	0.2
Fig. S1.10	2.0	726.8	12.75
Fig. S1.11	2.0	726.8	1.0
Fig. S1.12	2.0	726.8	0.2
Fig. S1.13	5.0	1338.9	17.67
Fig. S1.14	5.0	1338.9	1.0
Fig. S1.15	5.0	1338.9	0.2

TABLE S1.1. Parameters for the particle shape and wall proximity used in the fluctuating hydrodynamics calculations for ellipsoidal NCs in a cylindrical tube with $D = 5\,\mu$m and $L = 40\,\mu$m.

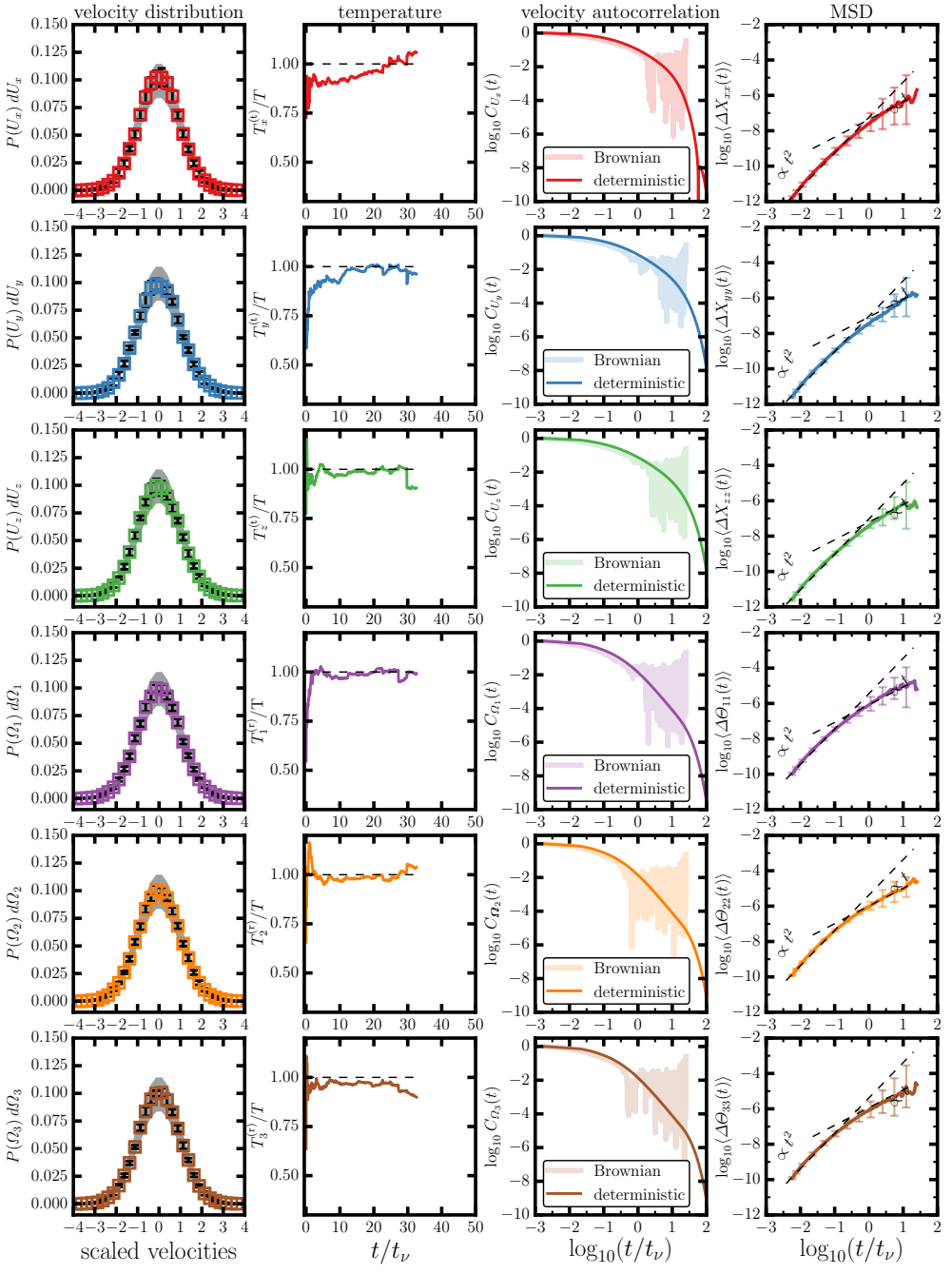

FIGURE S1.1. Oblate ellipsoid, with $\varepsilon = 0.5$ and $a = 288.4$ nm, at the center of a cylindrical tube, with $\widetilde{h} = 7.667$.

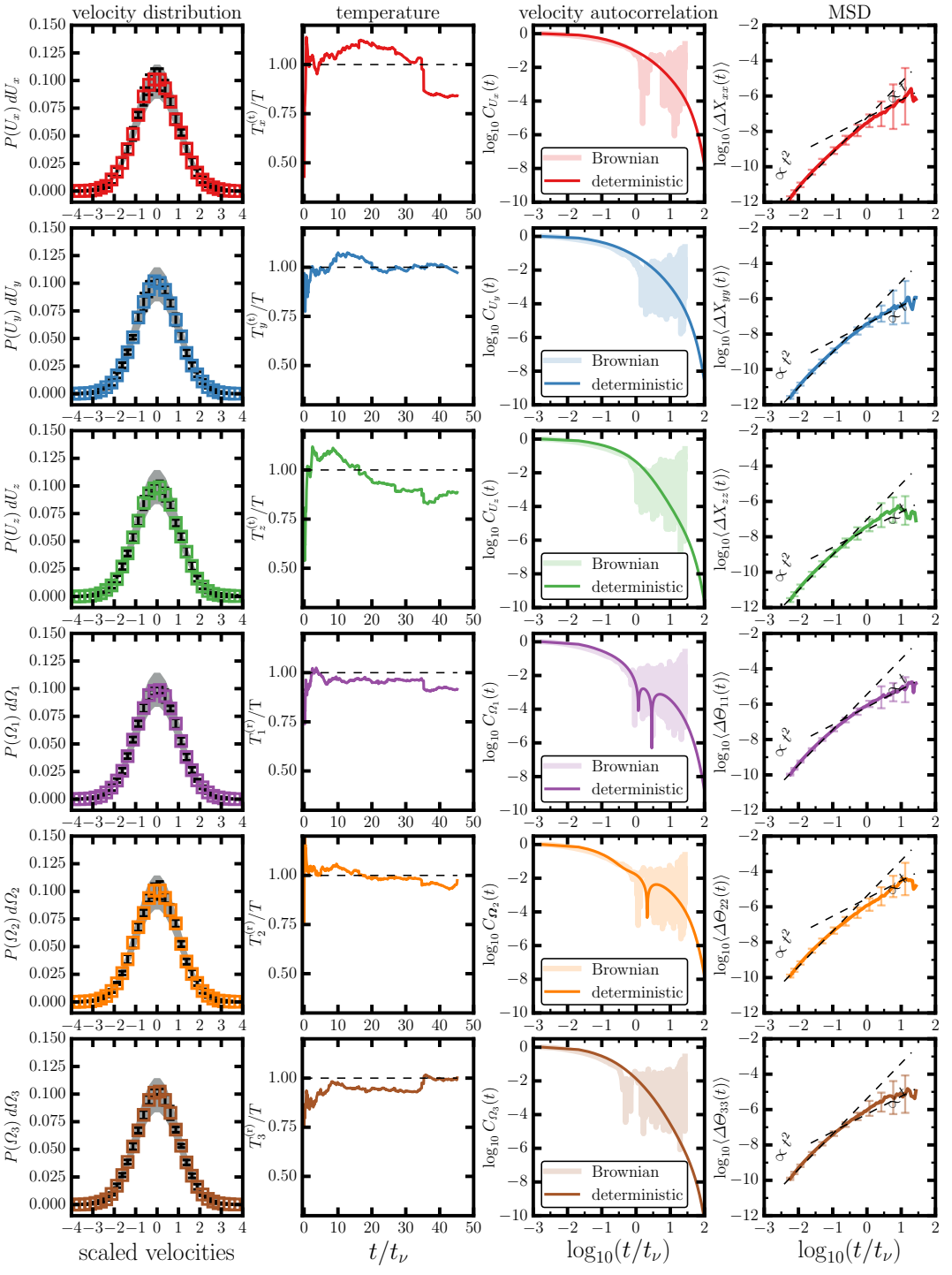

FIGURE S1.2. Oblate ellipsoid, with $\varepsilon = 0.5$ and $a = 288.4$ nm, placed close to the wall of a cylindrical tube, with $\widetilde{h} = 1$.

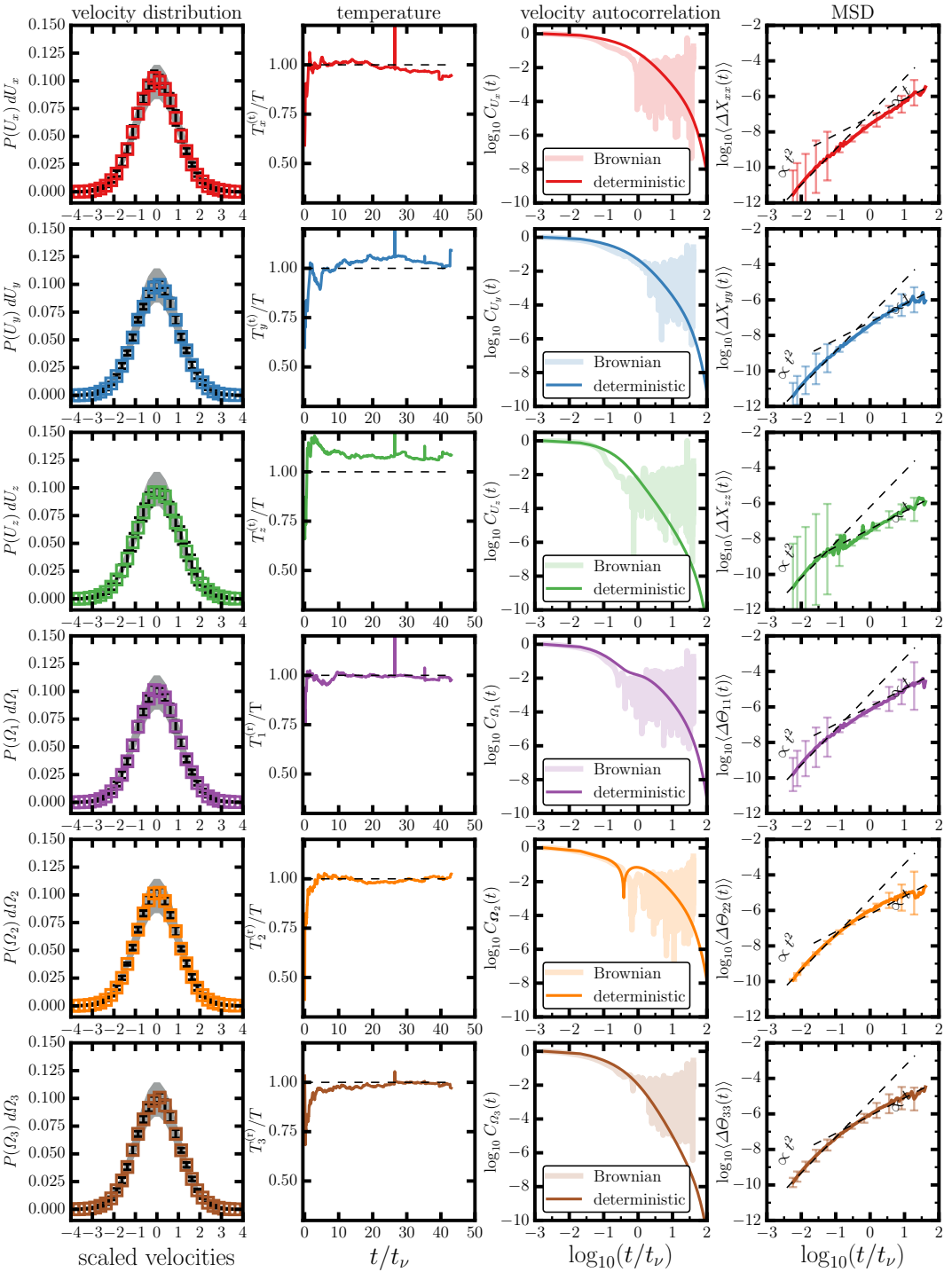

FIGURE S1.3. Oblate ellipsoid, with $\varepsilon = 0.5$ and $a = 288.4$ nm, placed in the lubrication layer of a cylindrical tube, with $\widetilde{h} = 0.2$.

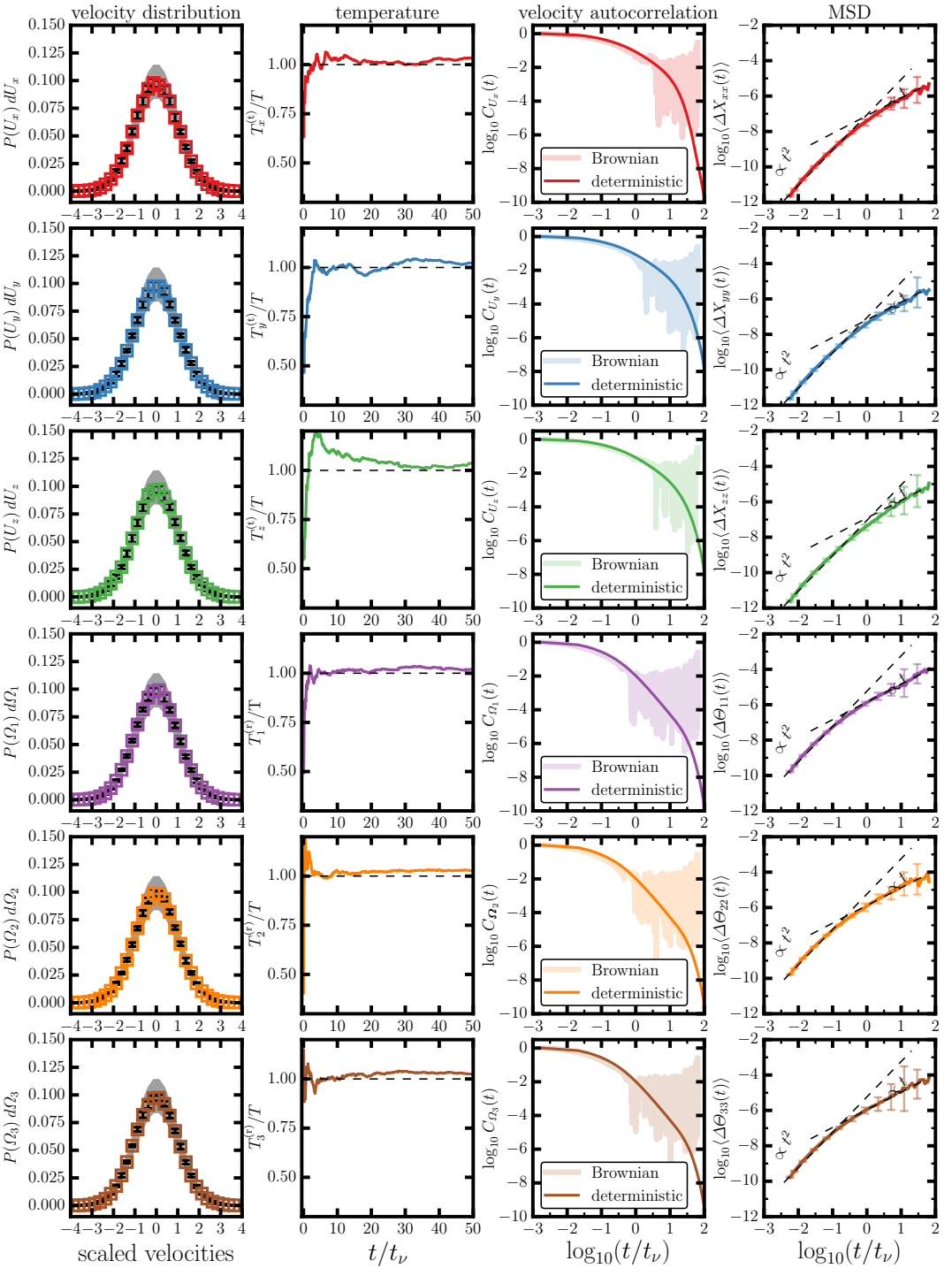

FIGURE S1.4. Spherical particle, with $\varepsilon = 1.0$ and $a = 457.9$ nm, at the center of a cylindrical tube, with $\widetilde{h} = 7.962$.

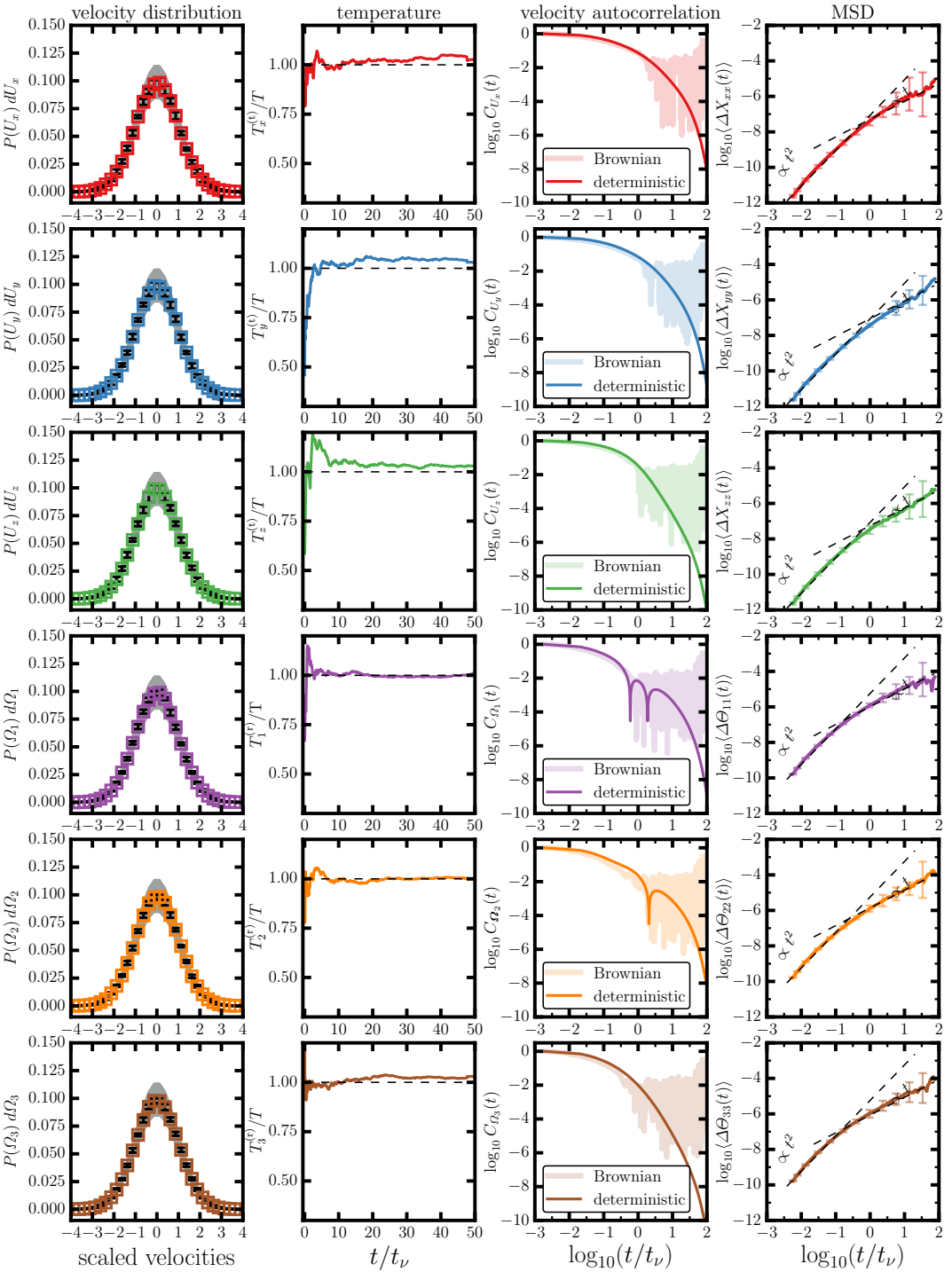

FIGURE S1.5. Spherical particle, with $\varepsilon = 1.0$ and $a = 457.9$ nm, placed close to the bounding wall of a cylindrical tube, with $\widetilde{h} = 1$.

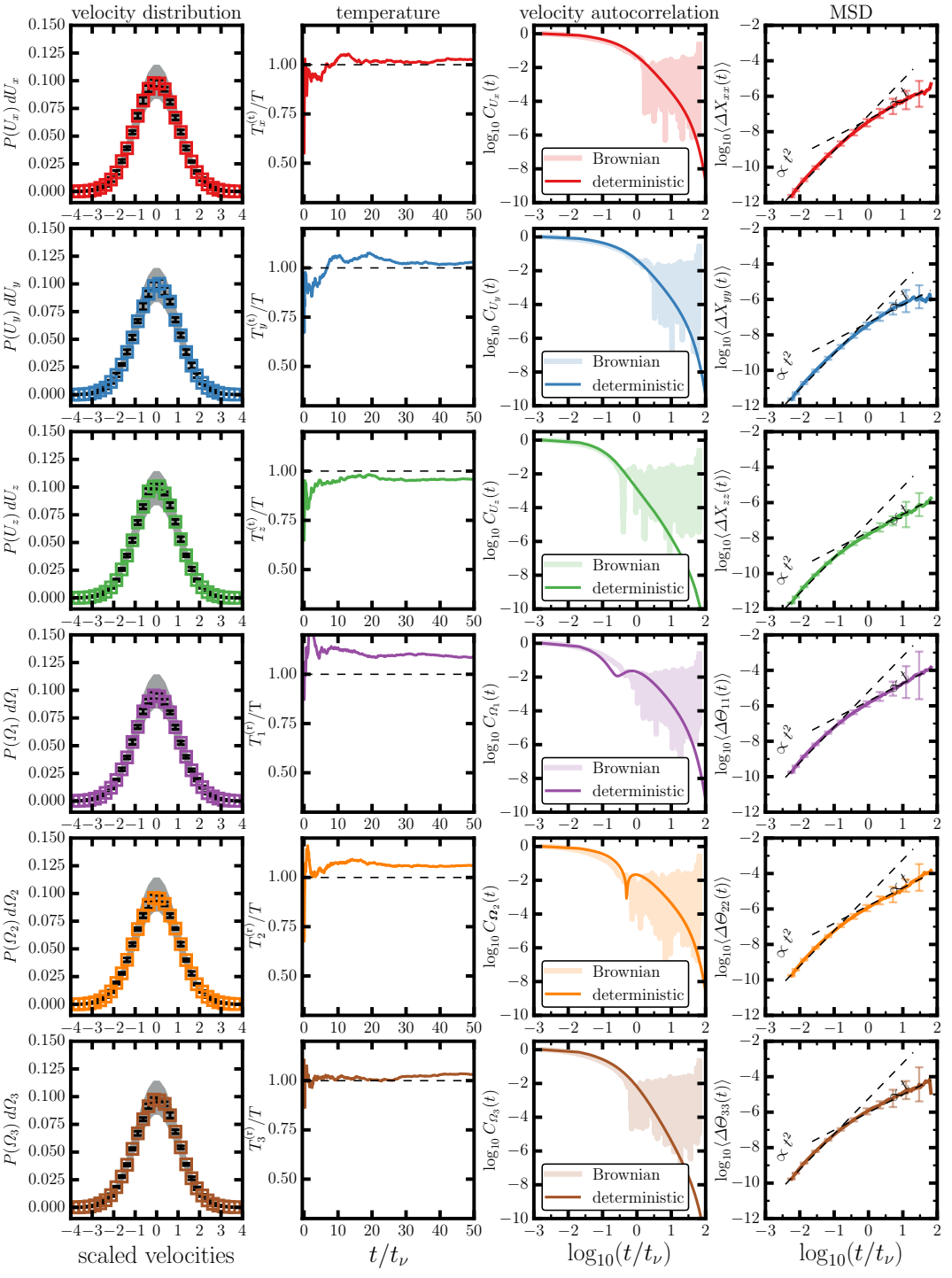

FIGURE S1.6. Spherical particle, with $\varepsilon = 1.0$ and $a = 457.9$ nm, placed in the lubrication layer of a cylindrical tube, with $\widetilde{h} = 0.2$.

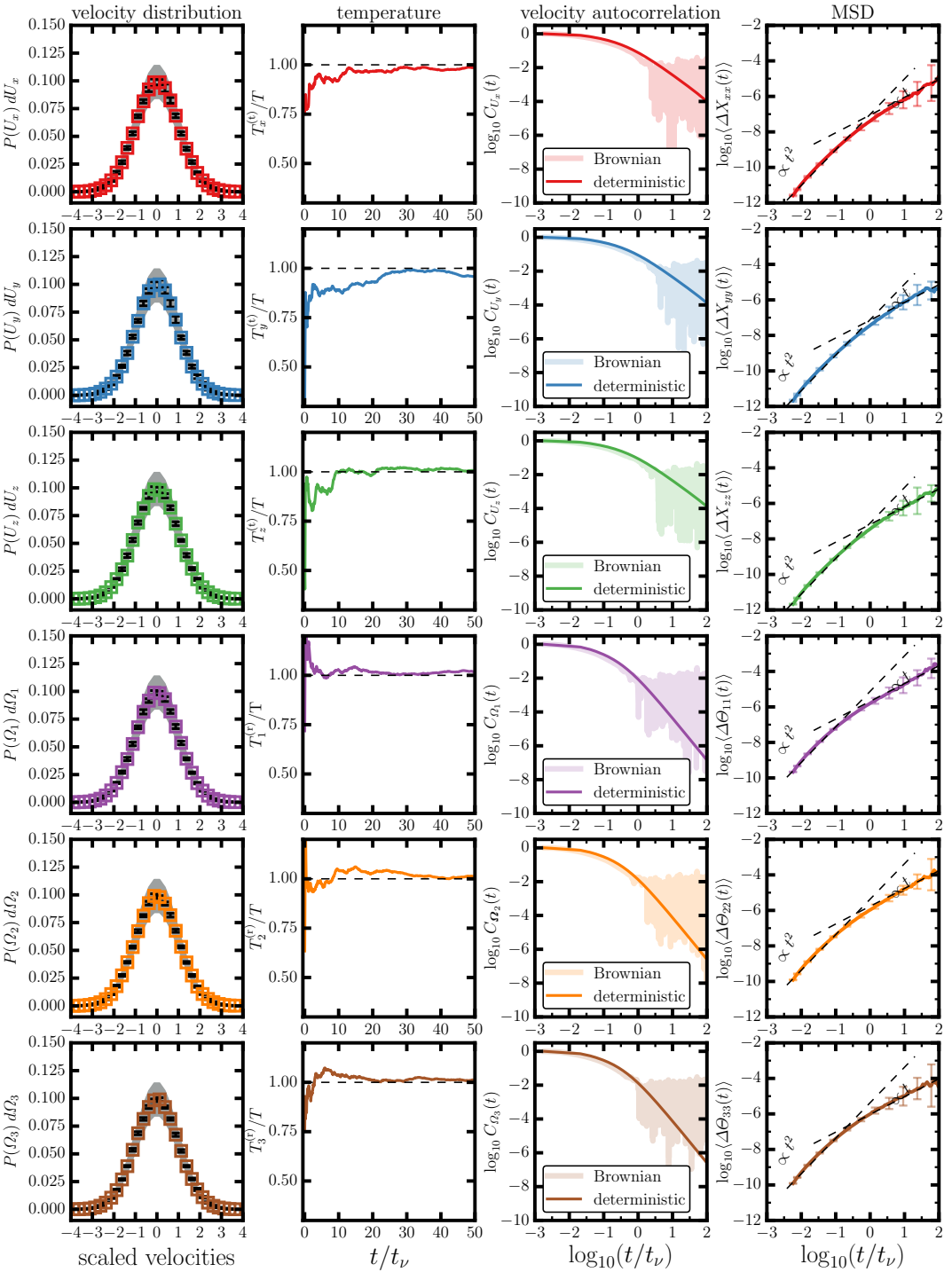

FIGURE S1.7. Spherical particle, with $\varepsilon = 1.5$ and $a = 600$ nm, at the center of a cylindrical tube, with $\widetilde{h} = 11.5$.

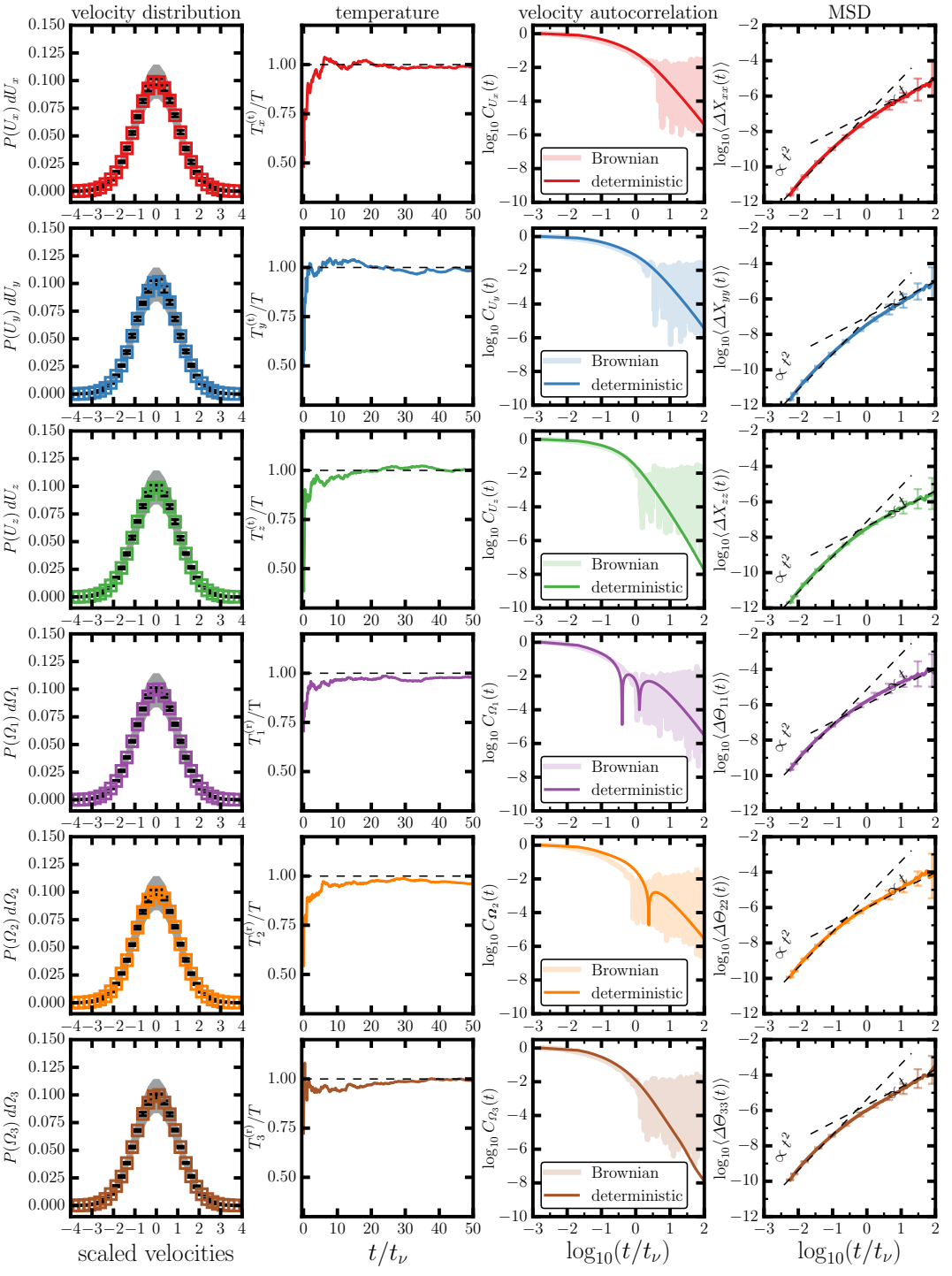

FIGURE S1.8. Spherical particle, with $\varepsilon = 1.5$ and $a = 600$ nm, placed close to the bounding wall of a cylindrical tube, with $\widetilde{h} = 1$.

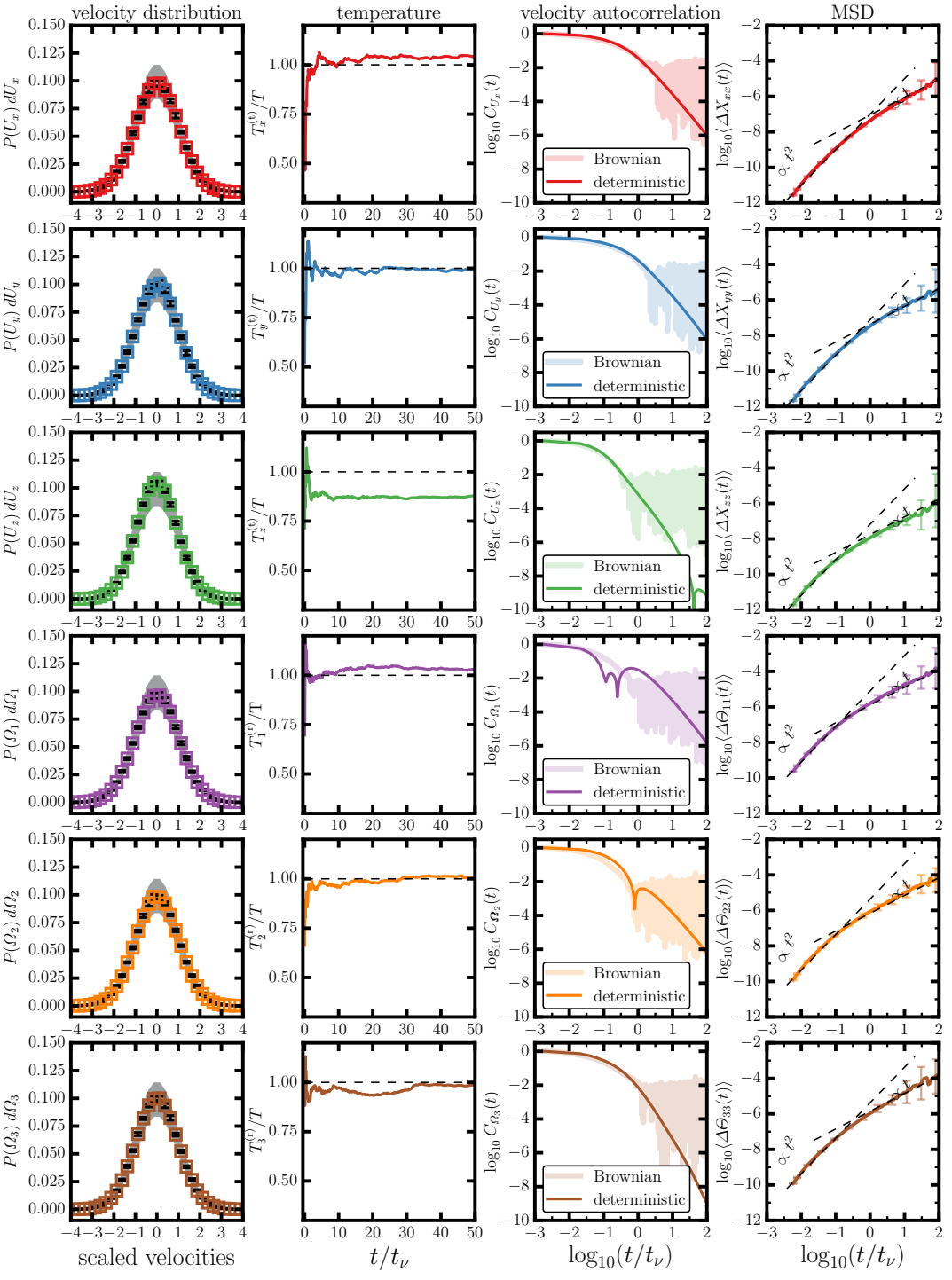

FIGURE S1.9. Spherical particle, with $\varepsilon = 1.5$ and $a = 600$ nm, placed in the lubrication layer of a cylindrical tube, with $\widetilde{h} = 0.2$.

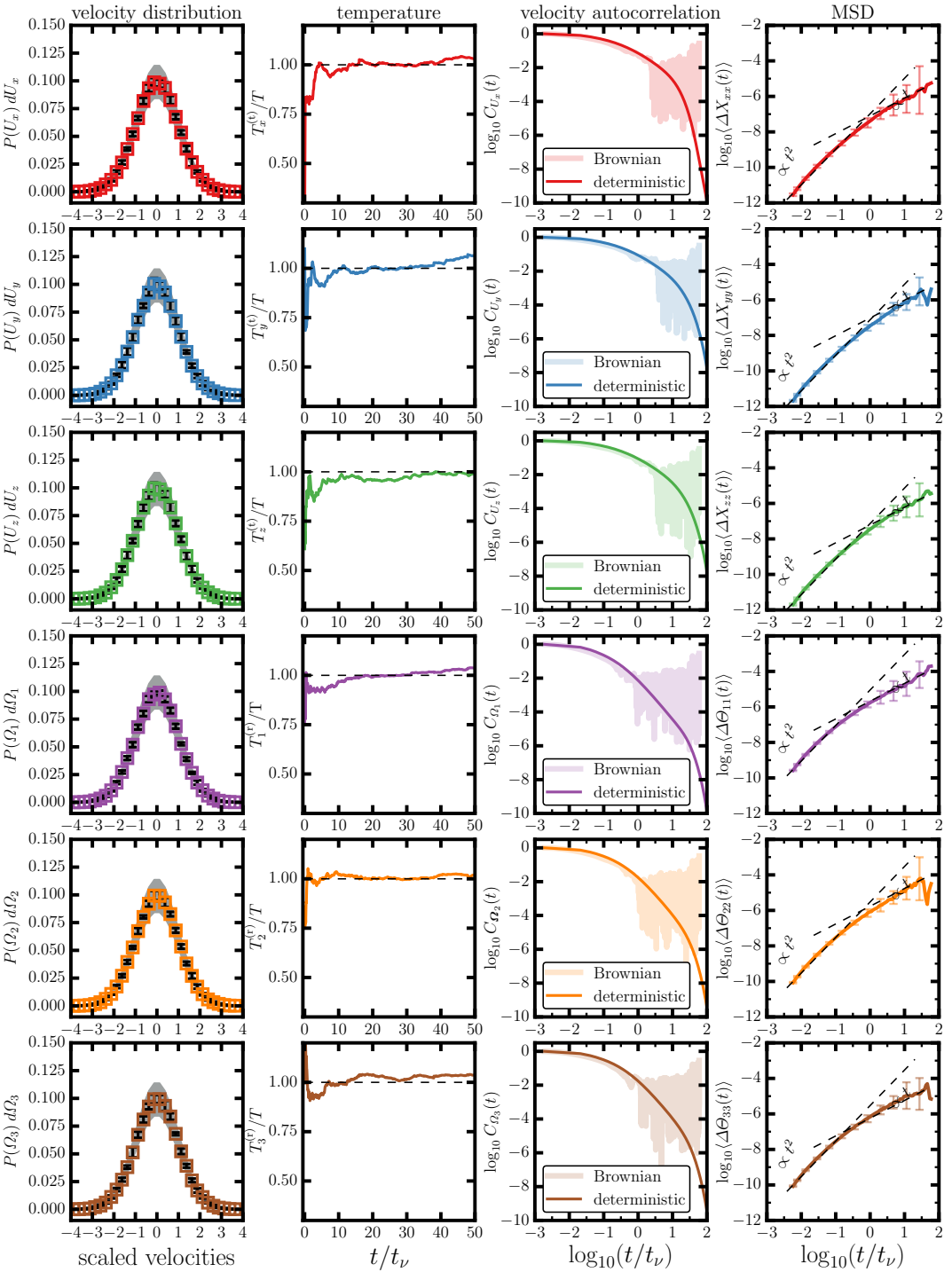

FIGURE S1.10. Prolate ellipsoid, with $\varepsilon = 2.0$ and $a = 726.8$ nm, at the center of a cylindrical tube, with $\widetilde{h} = 12.75$.

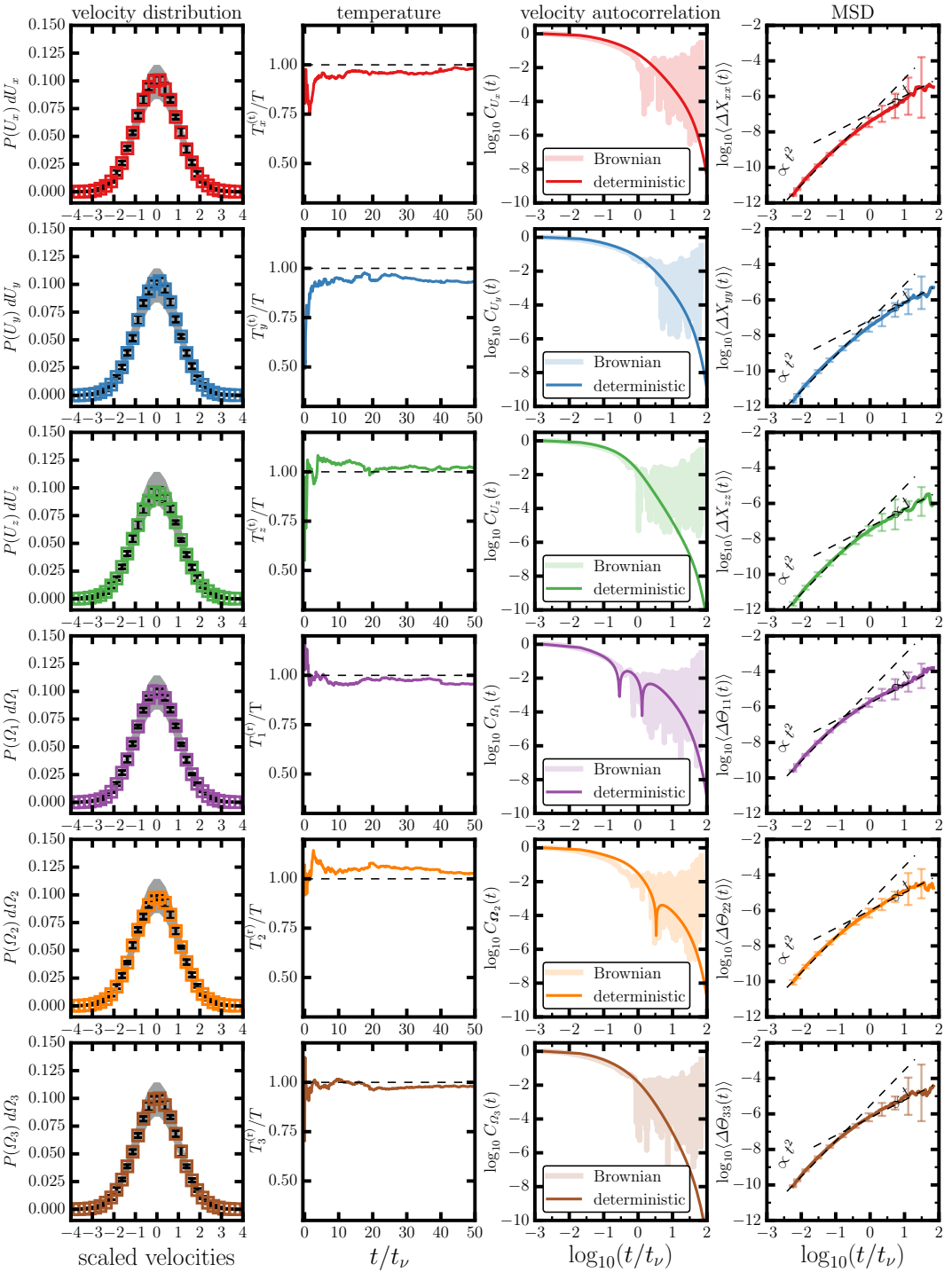

FIGURE S1.11. Prolate ellipsoid, with $\varepsilon = 2.0$ and $a = 726.8$ nm, placed in the near wall region of a cylindrical tube, with $\widetilde{h} = 1$.

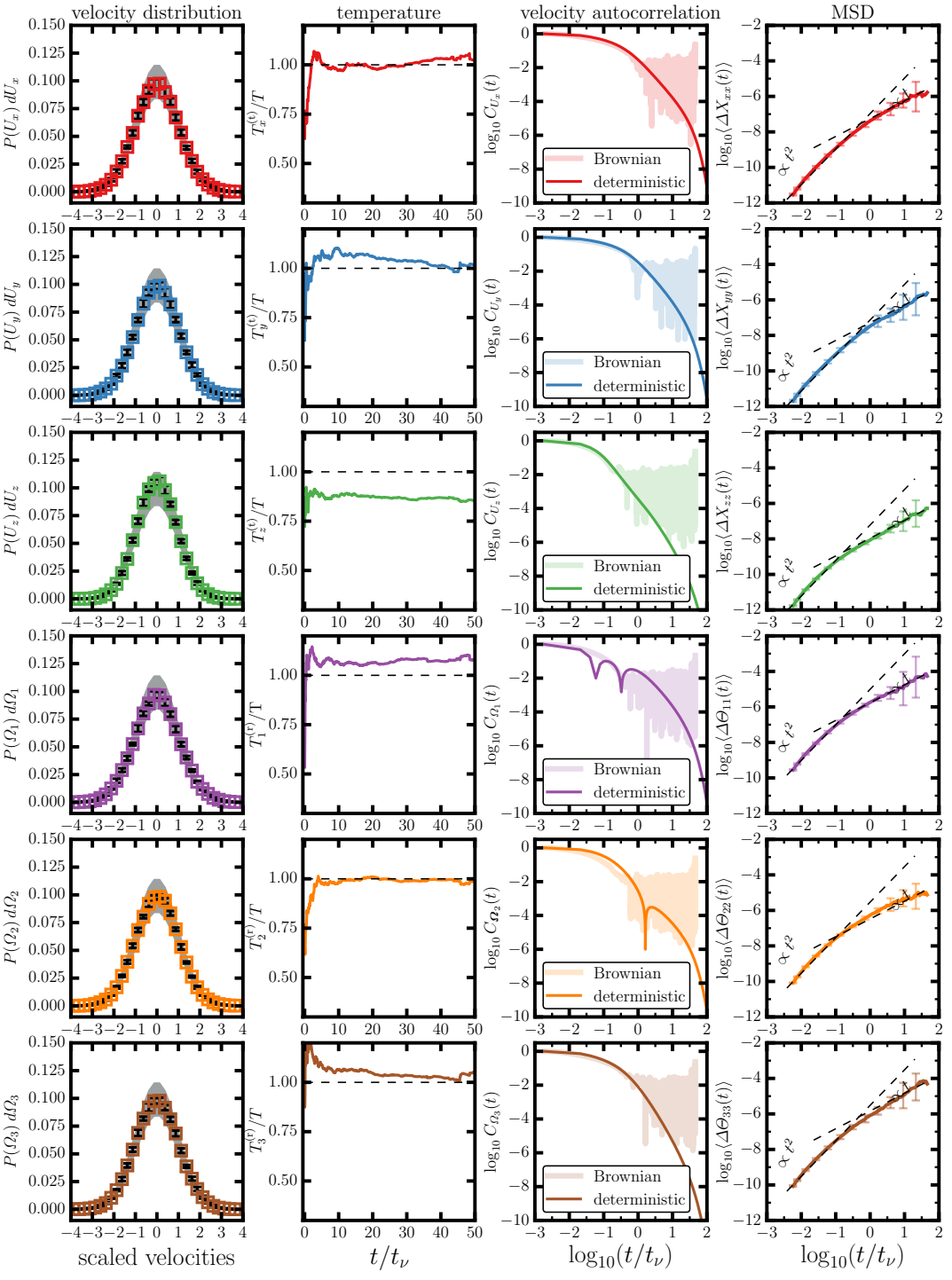

FIGURE S1.12. Prolate ellipsoid, with $\varepsilon = 2.0$ and $a = 726.8$ nm, placed in the lubrication layer of a cylindrical tube, with $\widetilde{h} = 0.2$.

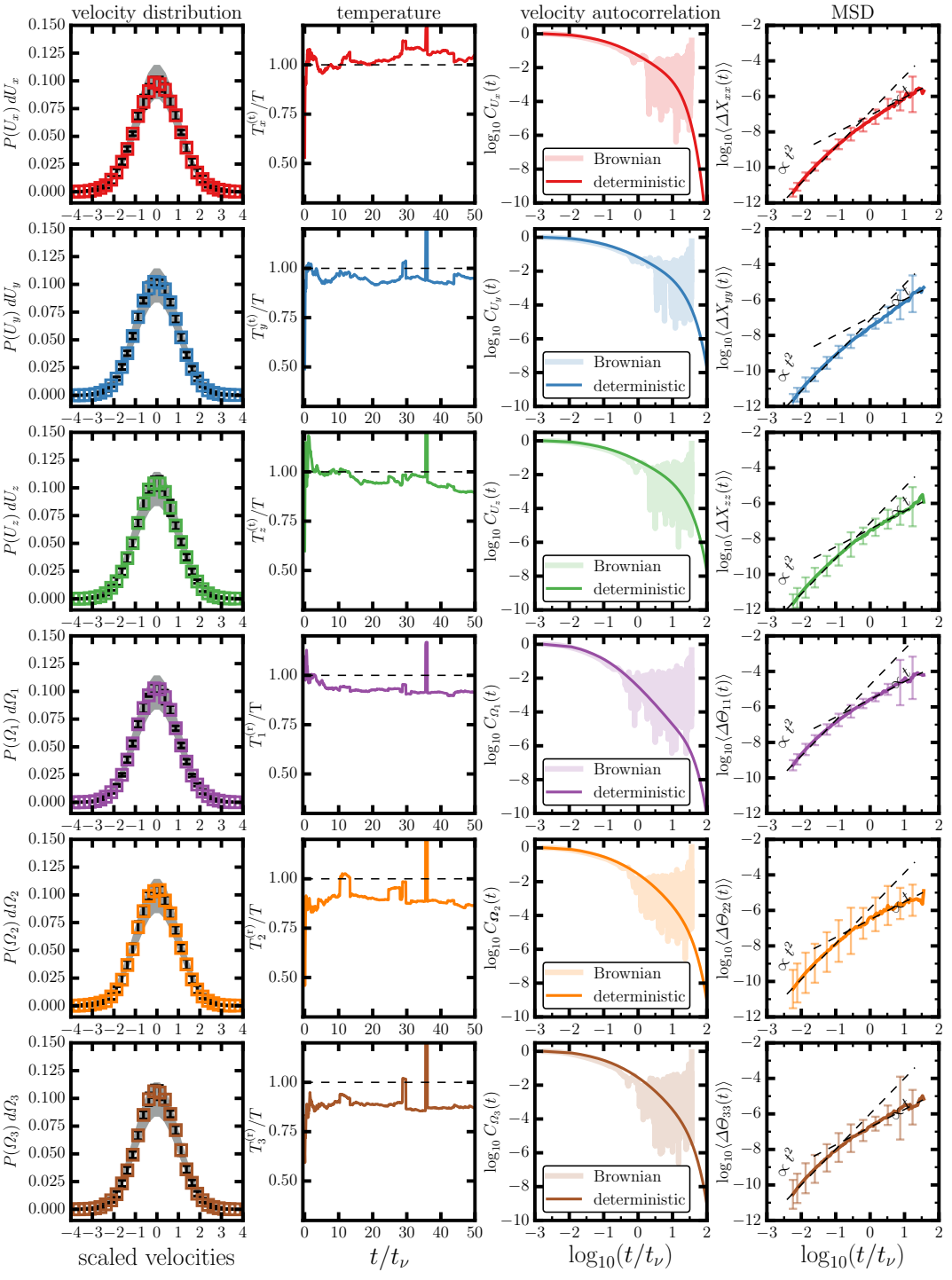

FIGURE S1.13. Prolate ellipsoid, with $\varepsilon = 5.0$ and $a = 1.3389\,\mu$m, at the center of a cylindrical tube, with $\widetilde{h} = 17.67$.

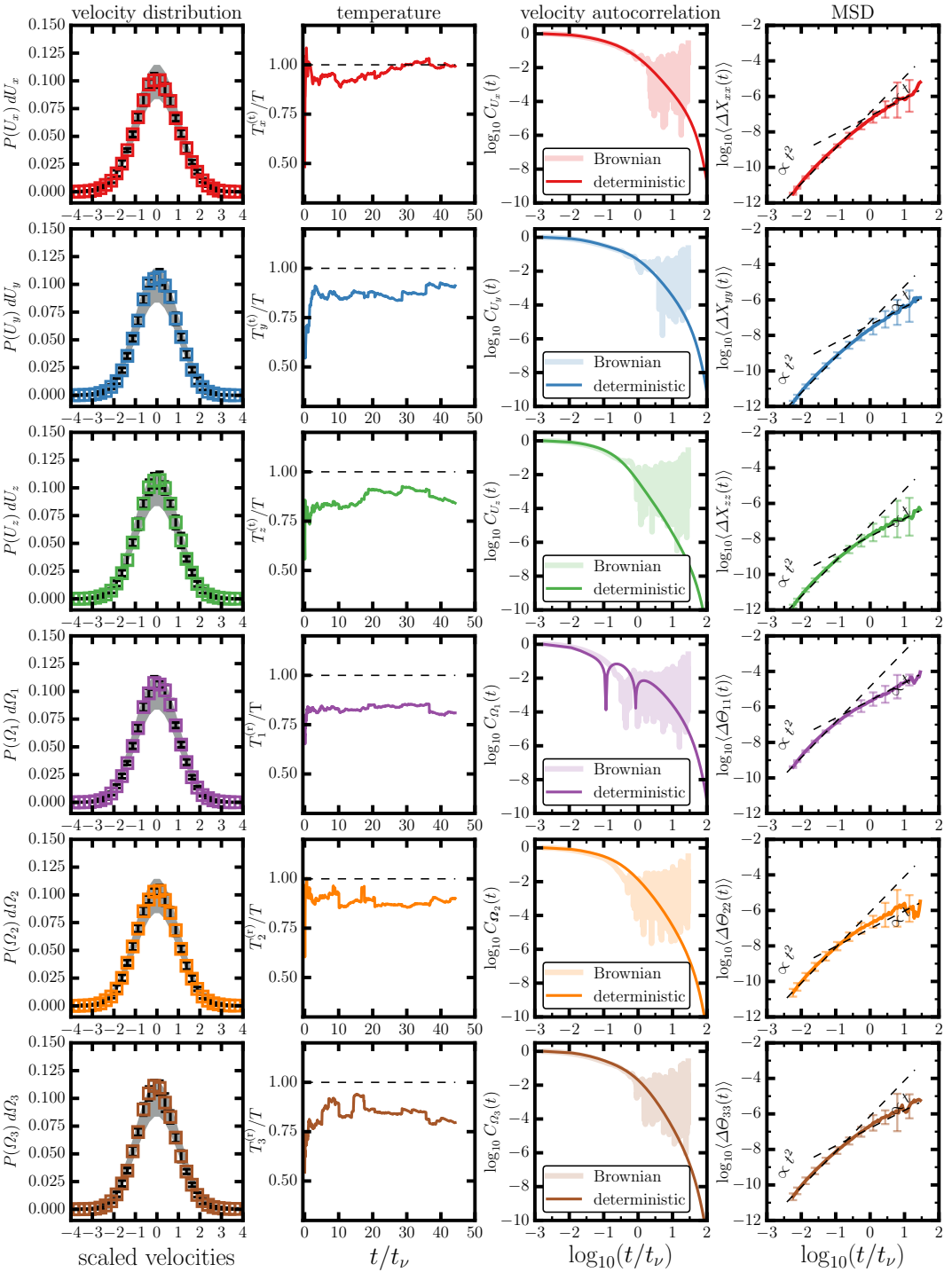

FIGURE S1.14. Prolate ellipsoid, with $\varepsilon = 5.0$ and $a = 1.3389\,\mu$m, in the near wall region of a cylindrical tube, with $\widetilde{h} = 1$.

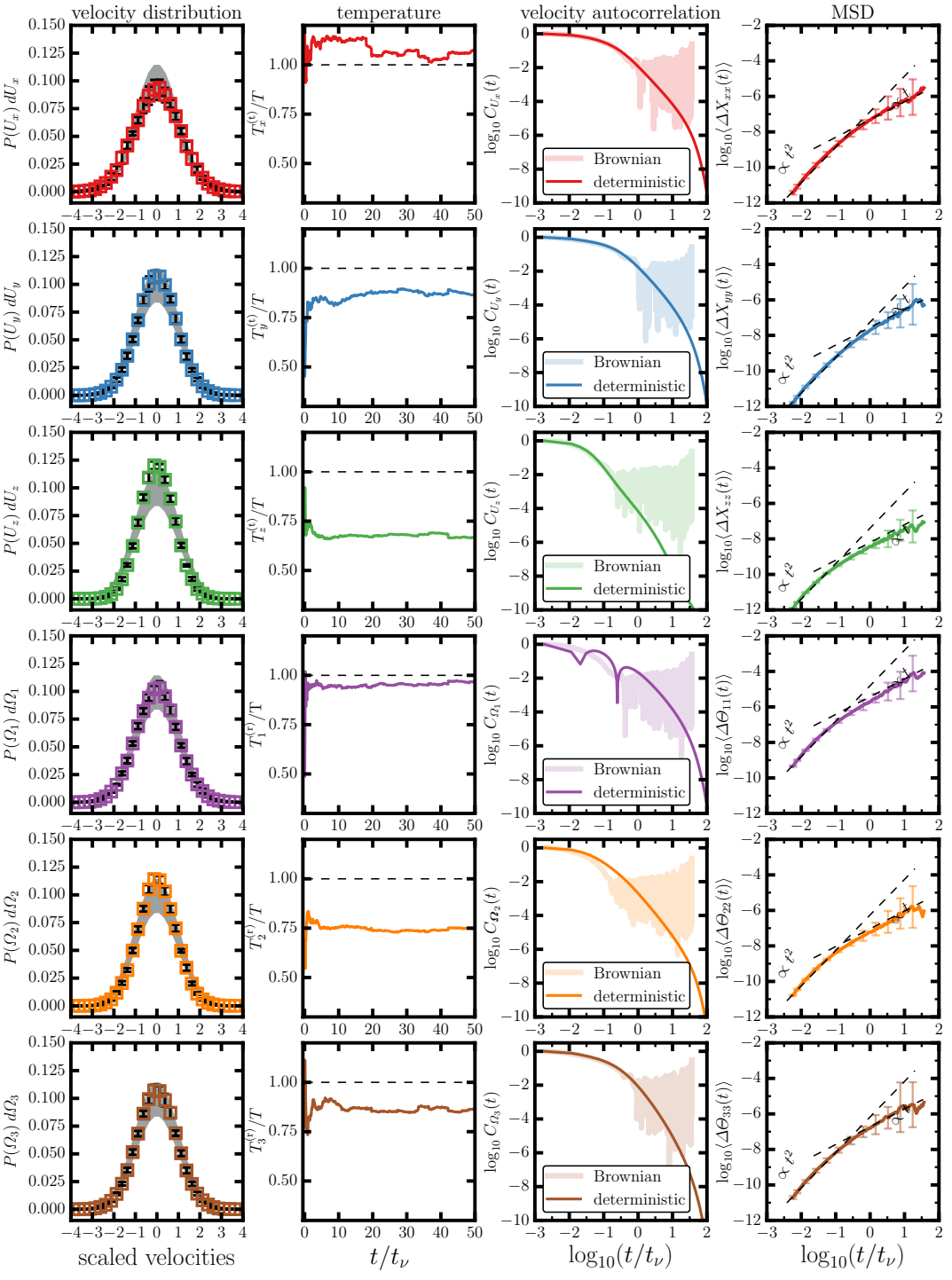

FIGURE S1.15. Prolate ellipsoid, with $\varepsilon = 5.0$ and $a = 1.3389\,\mu$m, placed in the lubrication layer of a cylindrical tube, with $\widetilde{h} = 0.2$.

S2. VACF and AVACF as a function of NC aspect ratio

In addition to its shape, the VACF and AVACF for an ellipsoidal NC are also strongly influenced by wall mediated hydrodynamic interactions when the NC is in proximity to the wall. A comparison of the VACF and AVACF are shown in Figs. S2.1 and S2.2, respectively, for NCs with ε=0.5, 1.0, 2.0, and 5.0 placed at $\widetilde{h} > 1.0$, $\widetilde{h} = 1.0$, and $\widetilde{h} = 0.2$ inside a cylindrical tube with $D = 5\,\mu$m and $L = 40\,\mu$m. These results have been used to compute the translational and rotational diffusivities presented in Figs.13 and 14 in the main text.

Furthermore, the curvature of the bounding wall may also alter the decay of the VACF and AVACF. This is shown in Figs. S2.3 and S2.4 for for NCs with ε=0.5, 1.0, 2.0 and 5.0 placed at $\widetilde{h} > 1.0$, $\widetilde{h} = 1.0$, and $\widetilde{h} = 0.2$ inside a cylindrical tube with $D = 20\,\mu$m and $L = 40\,\mu$m.

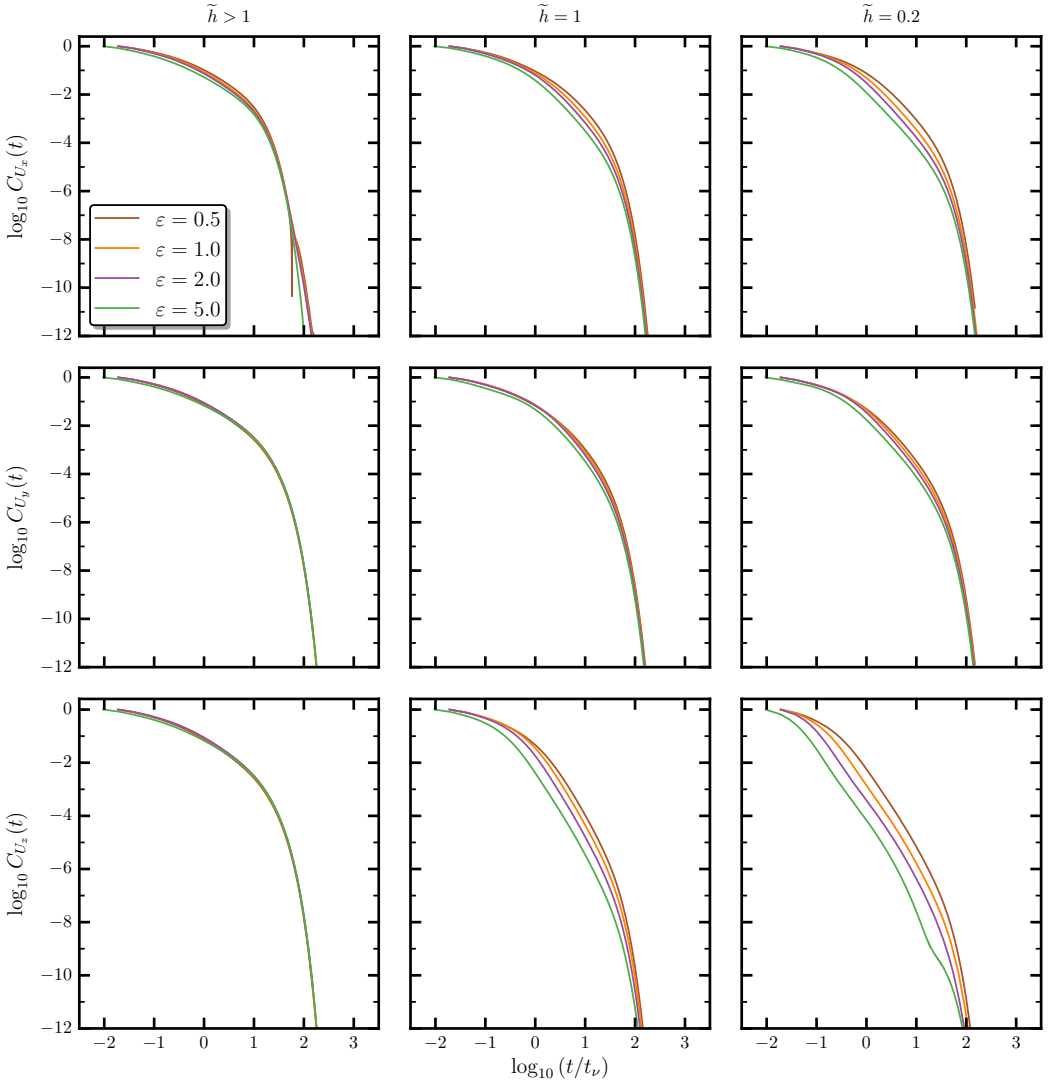

FIGURE S2.1. VACF for NCs with $\varepsilon = 0.5, 1.0, 2.0, 5.0$ placed at $\widetilde{h} > 1$ (see Table 1 in main text for exact values), $\widetilde{h} = 1$, and $\widetilde{h} = 0.2$, in a tube with $D = 5\,\mu$m and $L = 40\,\mu$m.

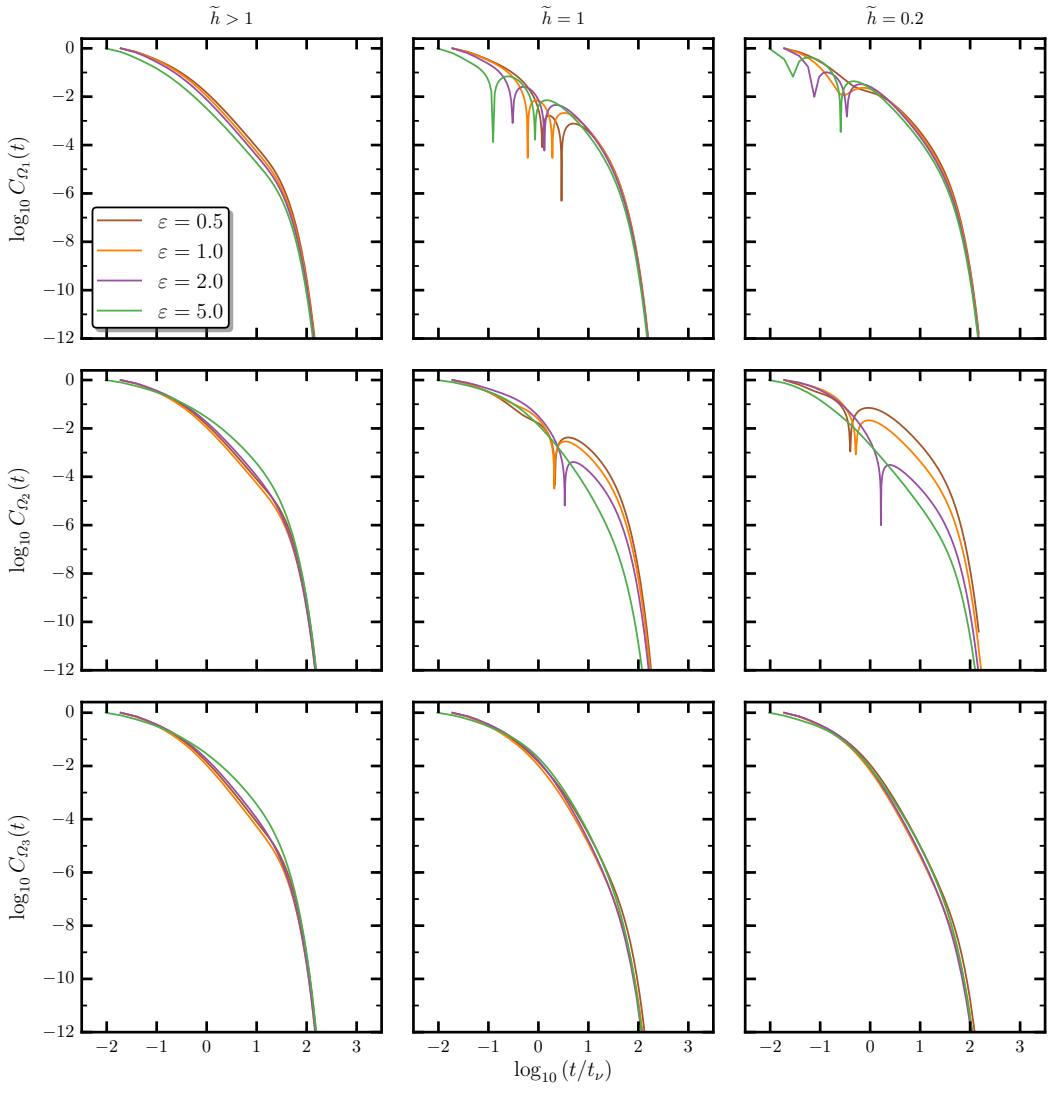

FIGURE S2.2. AVACF for NCs with $\varepsilon = 0.5, 1.0, 2.0, 5.0$ placed at $\widetilde{h} > 1$ (see Table 1 in main text for exact values), $\widetilde{h} = 1$, and $\widetilde{h} = 0.2$, in a tube with $D = 5\,\mu$m and $L = 40\,\mu$m.

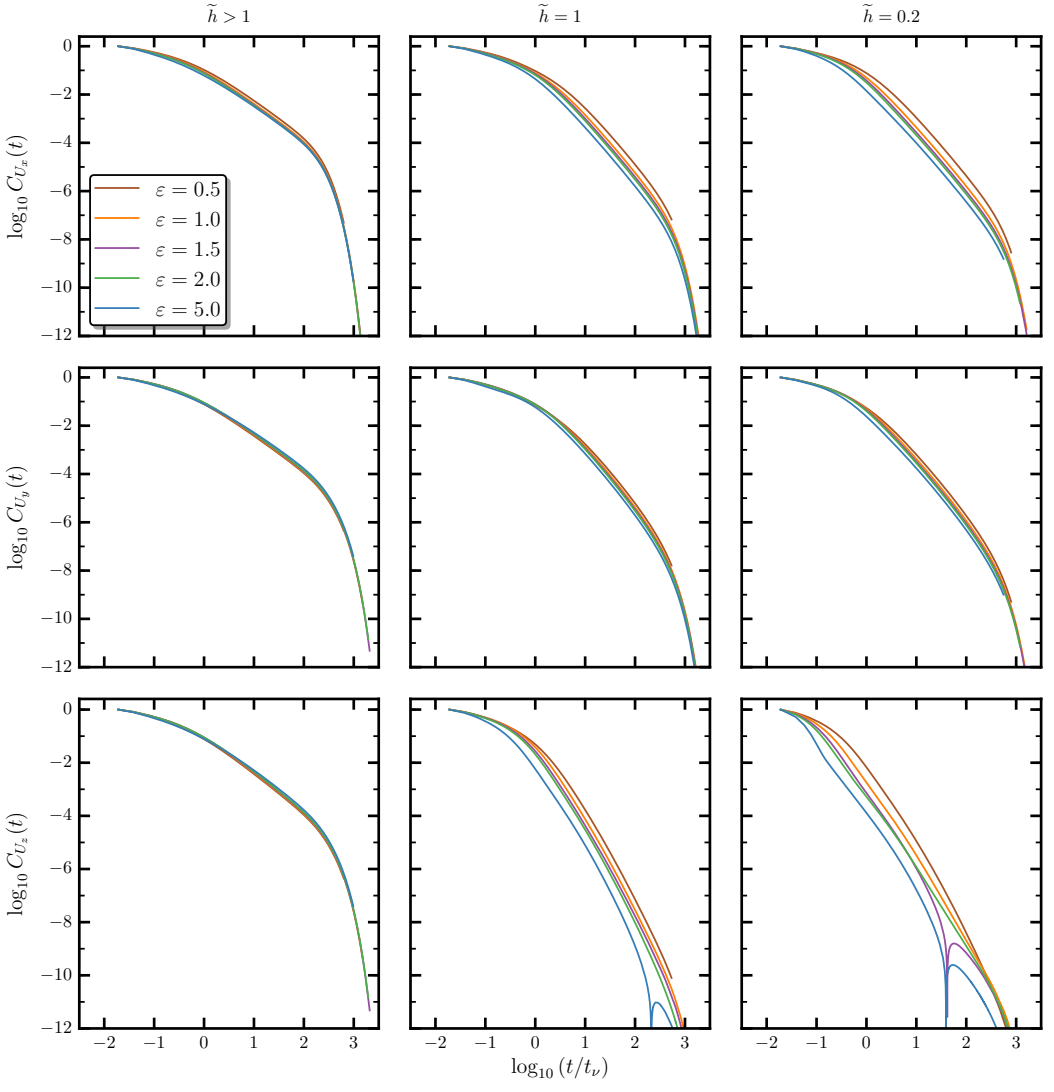

FIGURE S2.3. VACF for NCs with $\varepsilon = 0.5, 1.0, 2.0, 5.0$ placed at $\widetilde{h} > 1$ (see Table 1 in main text for exact values), $\widetilde{h} = 1$, and $\widetilde{h} = 0.2$, in a tube with $D = 20\,\mu$m and $L = 40\,\mu$m.

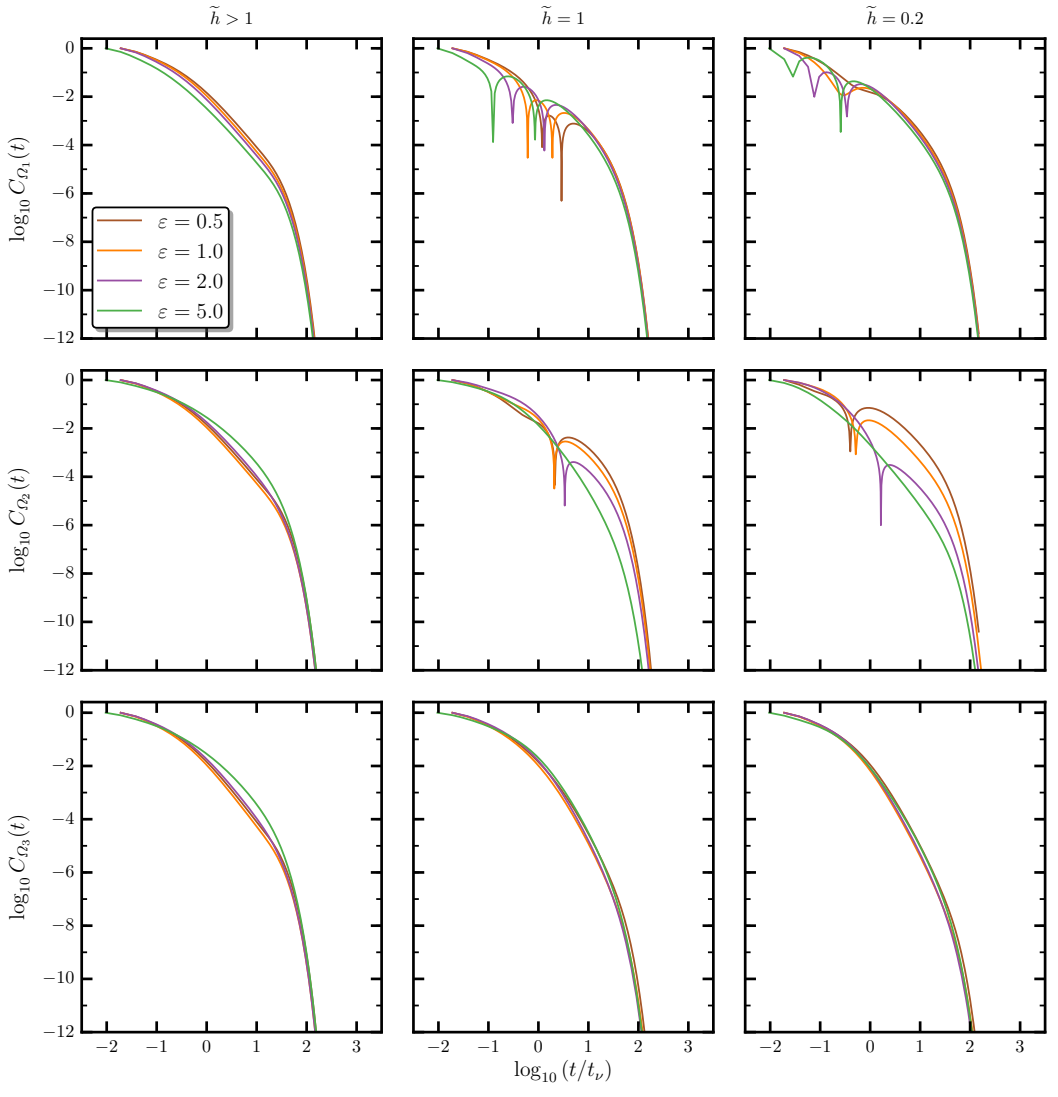

FIGURE S2.4. AVACF for NCs with $\varepsilon = 0.5, 1.0, 2.0, 5.0$ placed at $\widetilde{h} > 1$ (see Table 1 in main text for exact values), $\widetilde{h} = 1$, and $\widetilde{h} = 0.2$, in a tube with $D = 20\,\mu$m and $L = 40\,\mu$m.

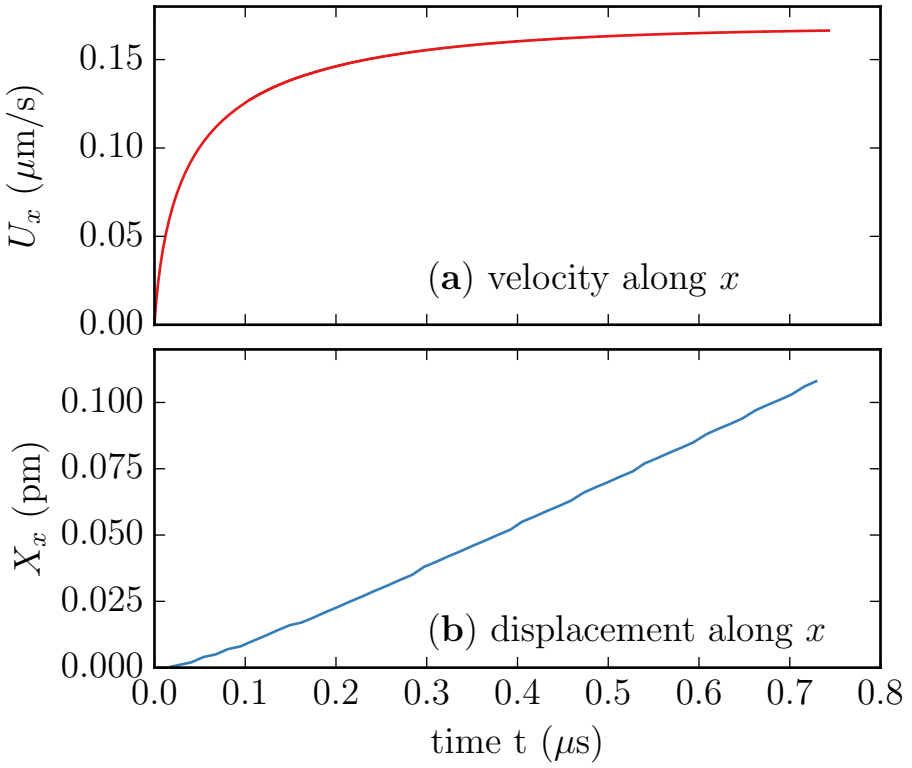

FIGURE S3.1. The time evolution of (a) the velocity and (b) the displacement of an ellipsoid with $\varepsilon = 1$ and $a = 500$ nm. The particle is placed at the center of a tube of diameter $D = 5\,\mu$m and is dragged along the x direction by applying a constant force $G_x = 10^{-18}$ N.

S3. Computing static mobilities using the Towing method

Here, we present a computationally inexpensive method to compute mobility of a neutrally buoyant ellipsoidal NC ($\rho^{(p)} = \rho^{(f)}$) by assessing the dynamics of the particle in response to a weak applied force. These calculations are performed with the weak formulation by setting the random stress tensor $\underline{\mathbf{S}}$, given in eqn. 3.3 in the main text, to zero.

The mobility of a nanoparticle $\mathcal{M}_\alpha$, at a radial position r and inclination angle θ as shown in Fig. 2(c), along any given direction α, is computed from its steady state velocity $\boldsymbol{U}$ in response to an externally imposed body force $\boldsymbol{G}$ (see eqn. 3.6) acting at its center of mass as $\mathcal{M}_\alpha = U_\alpha/G_\alpha$. Here, U_α and G_α are the components of the velocity and force along the α direction. In all the mobility calculations presented here, the force G_α is chosen to be $1\,\mathrm{pg}\,\mu\mathrm{m}\,\mathrm{s}^{-2}$. Figs. S3.1(a) and (b) show the time evolution of the x components of the velocity and displacement, used in computing $\mathcal{M}_x$ for a spherical particle (ellipsoid with $a = b = c$) of diameter 500 nm, placed at the center of a circular tube, and subjected to a constant force $G_x = 1\,\mathrm{pg}\,\mu\mathrm{m}\,\mathrm{s}^{-2} \equiv 10^{-18}$ N. It may be noted from these figures that the velocity reaches a steady state in a very short time ($\approx 10^{-6}$ ns). We ignore the initial transients and use the steady state value of U_x to compute the mobility. It should also be noted that the net displacement of the particle in the time interval to reach steady state is only about $10^{-11}\,\mu$m which is negligible compared to the particle diameter (500 nm). This method which neglects the transients

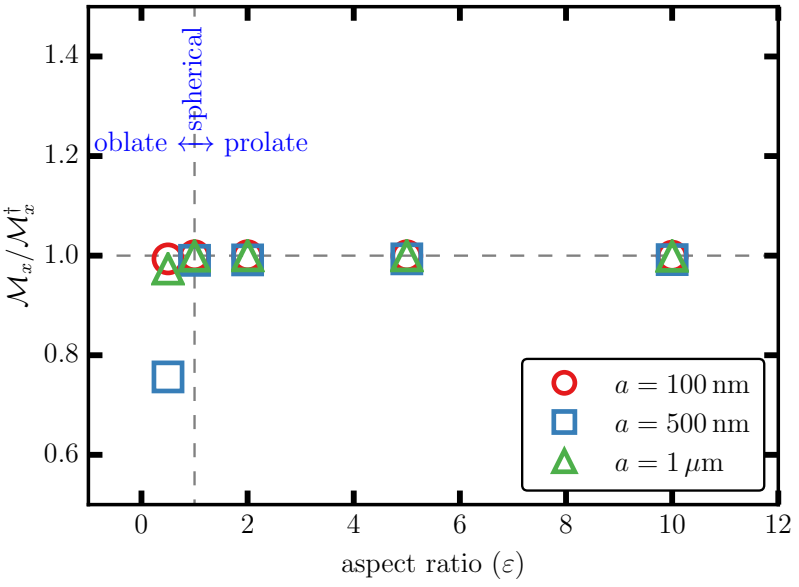

FIGURE S3.2. Comparison of the computed values of $\mathcal{M}_x$ to theoretical estimates based on eqn. (S3.1). Data shown as a function of the aspect ratio (ε) for ellipsoidal particles, with $a = 1\,\mu$m, 500 nm, and 100 nm, placed at the center of a tube with diameter $D = 5\,\mu$m. The normalization factor $\mathcal{M}_x^\dagger$, for each particle size a, is chosen to be the analytical estimate (from eqn. (S3.1)) for the corresponding spherical particle ($a = b = c$). Mesh parameters used are $l_P = 0.026\,\mu$m and $l_W = 0.524\,\mu$m.

and only probes the linear response regime of the particle allows us to compute the its zero-freqency mobility at the desired location.

Now we consider comparisons with existing results in two cases: (i) $\mathcal{M}_x$ as a function of the aspect ratio (ε) for an ellipsoid placed at the center of the cylindrical tube (Happel & Brenner 1965), and (ii) $\mathcal{M}_y$ for an ellipsoid as a function of its separation (h) from the tube wall (Hsu & Ganatos 1989).

For an ellipsoid particle (with $b = c$, and $\theta = 0°$) at the center of the tube ($r = 0$), the analytical form of the translational mobility $\mathcal{M}_x^\dagger$ is given by (Happel & Brenner 1965):

$$\mathcal{M}_x^\dagger = \frac{1 - \left(\frac{3d_{eq}}{8D}\right)\left(5.612 - 2.0211\left(\frac{a}{D}\right)^2 - 3.5431\left(\frac{c}{D}\right)^2\right)}{3\pi\mu d_{\mathrm{eq}}}. \tag{S3.1}$$

Here, d_{eq} is the "equivalent spherical diameter" for the ellipsoid, whose values have been taken from table 5-11.1 in Happel & Brenner (1965). We compare the values of $\mathcal{M}_x$ from our simulations to those evaluated from eqn. (S3.1) for particles with five different aspect ratios, ranging from $\varepsilon = 0.5$ to 10. We have chosen particles of three different sizes ($a = 1\,\mu$m, 500 nm, and 100 nm) and varied their aspect ratios by varying the values of b and c. In all these calculations we fix the cylindrical vessel diameter to be $D = 5\,\mu$m. Fig. S3.2 shows the ratio of $\mathcal{M}_x$ to $\mathcal{M}_x^\dagger$ and it may be seen that the computed values of the mobility are in excellent agreement with those given by eqn. (S3.1) and hence validate the computation for a particle situated away from the wall.

Next, we study the mobility of oblate ellipsoids with a fixed aspect ratio $\varepsilon = 0.5$, for $a = 100$ nm, 500 nm, and $1\,\mu$m, as a function of the gap length h between the center of mass of the particle and the tube wall (see Fig.2(c) in the main manuscript). These

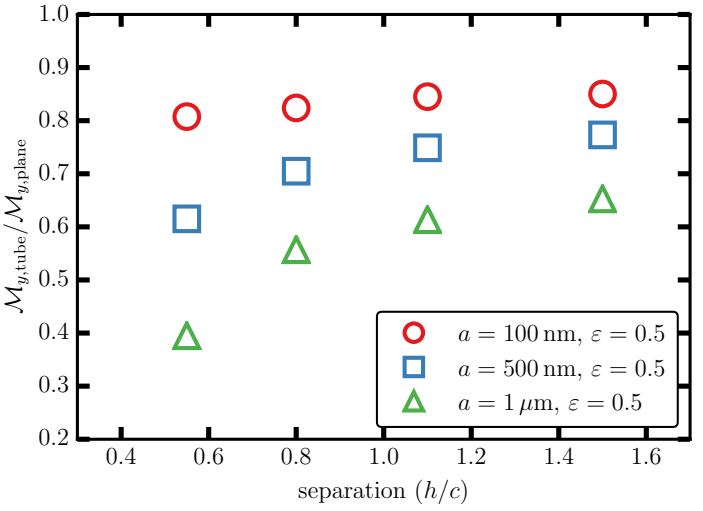

FIGURE S3.3. Ratio of the translational mobilities for an oblate ellipsoid in the vicinity of cylindrical and planar walls $\mathcal{M}_{y,\mathrm{tube}}/\mathcal{M}_{y,\mathrm{plane}}$. Data shown as a function of the particle separation from the wall h, and in our simulations h is varied by varying the particle position along the y direction. The estimates for $\mathcal{M}_{y,\mathrm{plane}}$ is from Hsu and Ganatos (Hsu & Ganatos 1989). We consider three different ellipsoidal particles with a fixed $\varepsilon = 0.5$ and $a = 100$ nm, 500 nm and $1\,\mu$m, in a cylindrical tube diameter of $D = 5\ \mu$m. Mesh parameters for the particle surface are $l_P = 6$ nm, 16 nm, and 64 nm for the 100 nm, 500 nm, and $1\,\mu$m particles, respectively, and $l_W = 524$ nm for the mesh on the cylindrical wall.

studies have been performed by varying h along the y direction for an ellipsoidal particle whose axis of symmetry is also oriented along y (i.e., $\theta = 90°$). This study will validate the numerical scheme where the wall effects are important. Hsu and Ganatos (Hsu & Ganatos 1989) have previously reported a similar study using the boundary integral approach to compute the mobility of an ellipsoidal particle as a function of its separation from a plane wall.

A comparison of results are shown in Fig. S3.3 where we have plotted the ratio $\mathcal{M}_{y,\mathrm{tube}}/\mathcal{M}_{y,\mathrm{plane}}$ as a function of h/c. For a particle located at the center of the tube, the effect of wall curvature is a minimum and hence, $\mathcal{M}_{y,\mathrm{tube}}/\mathcal{M}_{y,\mathrm{plane}} \simeq 1$. Indeed, this is displayed in Fig. S3.3. For locations closer to the wall boundary, the curvature effects would become increasingly important as we approach the wall. Again, as displayed in Fig. S3.3 the ratio of the mobilities shows significant deviation from unity as we approach the wall and this effect is more pronounced with increasing particle size. This is as would be expected. These complete our validations.

S3.1. *Effects of the bounding geometry and particle orientation in the absence of Brownian stresses*

In order to quantify the effects of the wall curvature and the particle orientation, we have computed the mobility of an ellipsoidal particle ($a = 0.6\,\mu$m and $b = c = 0.4\,\mu$m) placed at three different positions of the center of mass along the radial direction chosen as $r = 0.0\,\mu$m , $r = 1.9\,\mu$m, and $r = 2.1\,\mu$m, which are representative of a particle in the bulk, near wall and lubrication regimes, for various inclination angles $0 \leqslant \theta \leqslant 90$. The mobility calculations are performed as described earlier for both quiescent and Poiseuille flow conditions. For the Poiseuille flow, $\boldsymbol{u}_{\mathrm{in}}(r) = u_{\max}\left(1 - (2r/D)^2\right)\hat{\boldsymbol{x}}$, where $u_{\max}$ is the flow velocity at the center of the tube, and D denotes the diameter of the tube. In

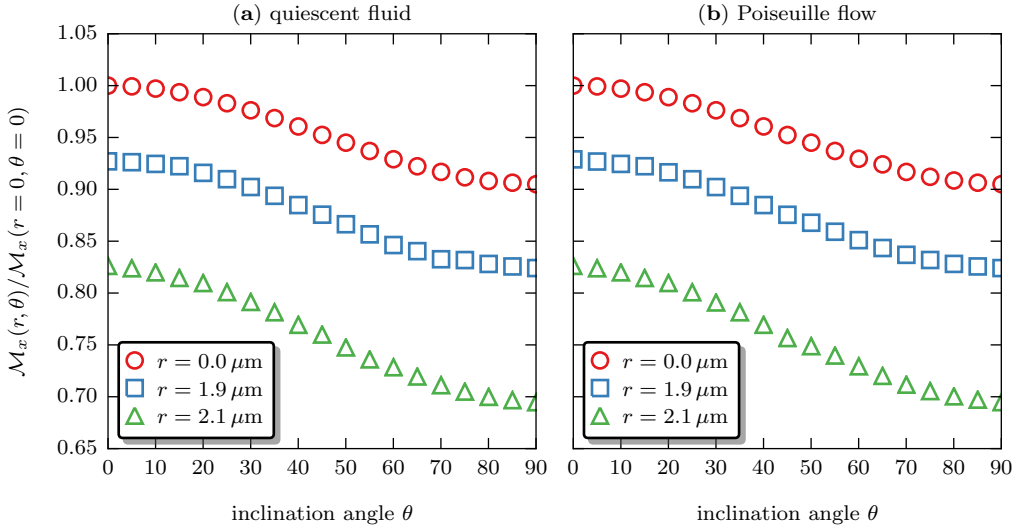

FIGURE S3.4. The normalized mobility for an ellipsoidal particle, with $\varepsilon = 1.5$ and $a = 500$ nm, as a function of its inclination angle θ for three different radial positions – (i) center ($r = 0.0$ μm), (ii) near wall ($r = 1.9$ μm), and (iii) lubrication ($r = 2.1$ μm) – in (a) a quiescent medium and (b) a Poiseuille flow field. Mesh parameters used are $l_P = 5$ nm and $l_W = 785$ nm.

targeted drug delivery applications since we are interested in capillary flows, we have performed our simulations with $u_{\max} = 0.1\,\mathrm{cm/s}$, which is representative of flow rates in capillary vessels (Mazumdar 1992). Figures S3.4(a) and (b) show ratio of the mobilities ($\mathcal{M}_x(r,\theta)/\mathcal{M}_x(r=0,\theta=0)$) of the ellipsoid as a function of θ and its separation from the wall. We find that the mobility of the particle is strongly dependent both on the orientation θ and its radial position r. The effect of the flow field of the mobility is weak due to the low particle Reynolds number considered here ($\mathrm{Re}^{(p)} \sim 10^{-4}$).

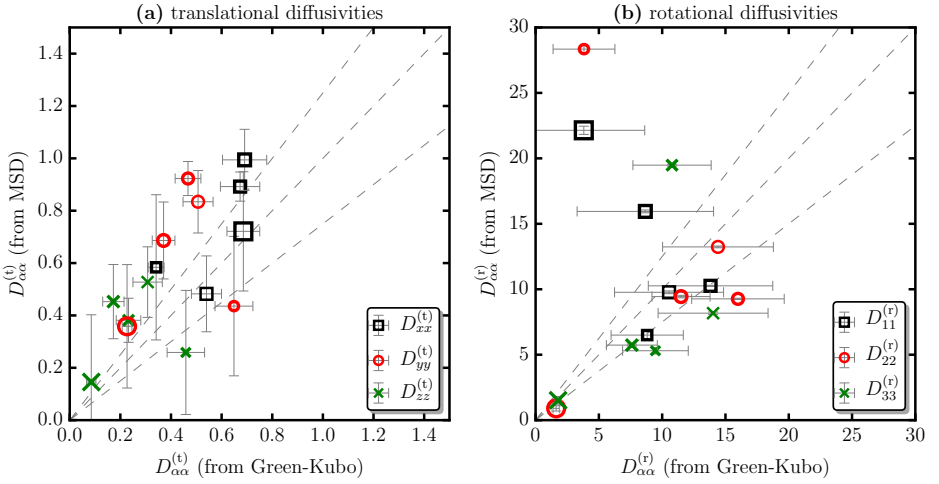

FIGURE S4.1. Comparison of the translational and rotational diffusivities computed from the velocity-autocorrelation, using the Green-Kubo relation, to those estimated from the MSDs. Data for shown for NCs with five different aspect ratios and placed at $\widetilde{h} = 1.0$. The central dotted line represents the linear correlation while the rest two represent deviations of $\pm 20\%$. The translational diffusivities (panel (a)) are in units of $\mu\text{m}^2\text{s}^{-1}$, and the rotational diffusivities (panel (b)) are in units of $\text{rad}^2\text{s}^{-1}$.

S4. Comparison of diffusivities for $\widetilde{h} = 1$ and $\widetilde{h} = 0.2$

Figs. S4.1 and S4.2 show a comparison of the translational and rotational diffusivities for ellipsoidal NCs (with ε=0.5, 1.0, 1.5, 2.0, and 5.0) computed using the MSD approach and from the VACF, using the Green-Kubo relation, for $\widetilde{h} = 1.0$ and $\widetilde{h} = 0.2$, respectively. Data correspond to ellipsoidal NCs in a tube with $D = 5\,\mu\text{m}$ and $L = 40\,\mu\text{m}$.

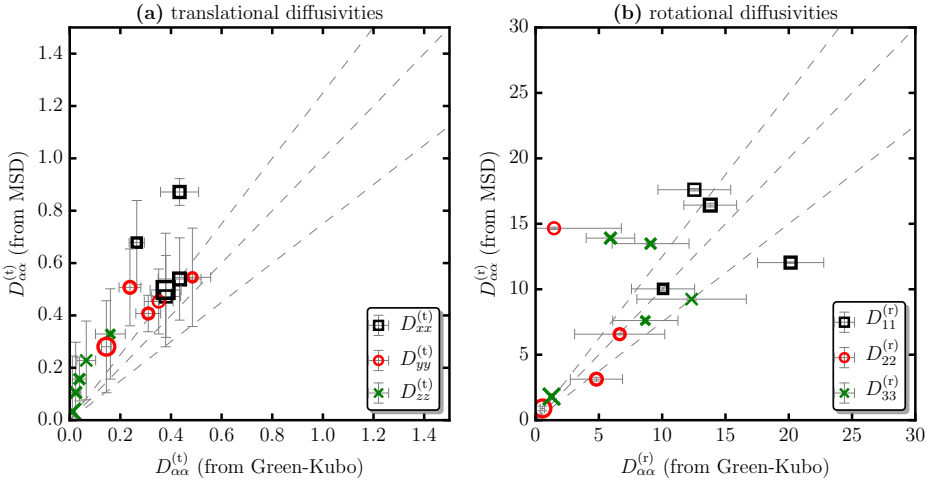

FIGURE S4.2. Comparison of the translational and rotational diffusivities computed from the velocity-autocorrelation, using the Green-Kubo relation, to those estimated from the MSDs. Data for shown for NCs with five different aspect ratios and placed at $\widetilde{h} = 0.2$. The central dotted line represents the linear correlation while the rest two represent deviations of $\pm 20\%$. The translational diffusivities (panel (a)) are in units of $\mu\text{m}^2\text{s}^{-1}$, and the rotational diffusivities (panel (b)) are in units of $\text{rad}^2\text{s}^{-1}$.

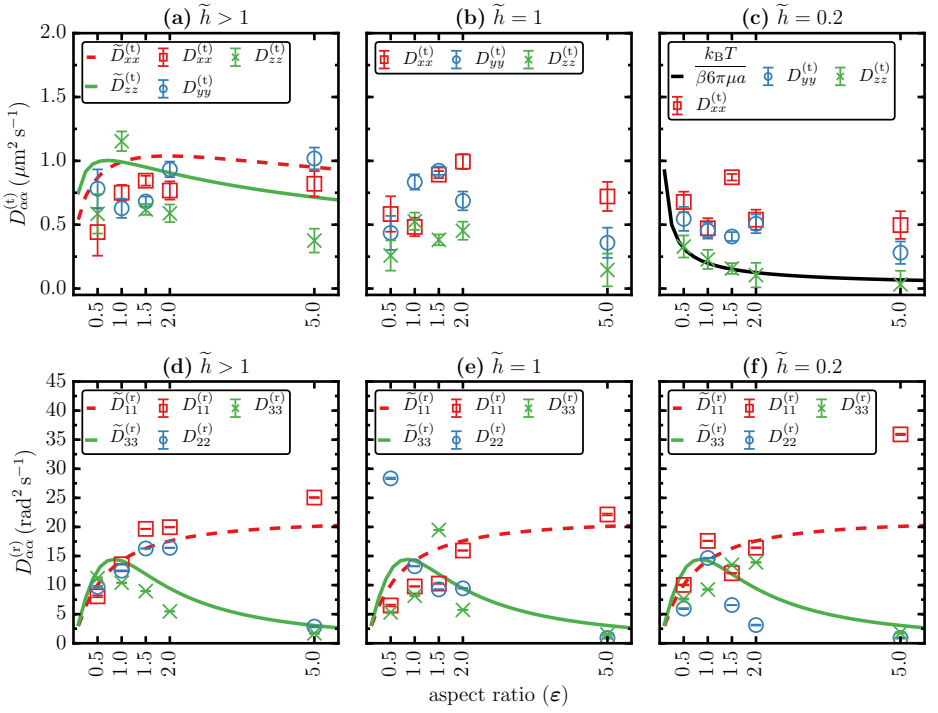

FIGURE S5.1. Translational and rotational MSDs estimated from the MSD, as a function of the aspect ratio and $\widetilde{h}$. The dotted and solid lines in the various panels are as described in Fig.14 in the main text.

S5. Comparison of diffusion constants estimated from MSD

In Fig. S5.1, we show the scaling behavior of the translational and rotational diffusivities computed using the MSD approach, as functions of ε and $\widetilde{h}$. For a detailed description of the various scaling behavior see discussions around Fig. 14 in the main text.

REFERENCES

HAPPEL, J. & BRENNER, H. 1965 *Low Reynolds Number Hydrodynamics*. Prentice Hall.

HSU, R. & GANATOS, P. 1989 The motion of a rigid body in viscous fluid bounded by a plane wall. *Journal of Fluid Mechanics* **207**, 29–72.

MAZUMDAR, J. N. 1992 *Biofluid Mechanics*. World Scientific.